processes

MDPI

Article

Keller-Box Simulation for the Buongiorno Mathematical Model of Micropolar Nanofluid Flow over a Nonlinear Inclined Surface

Khuram Rafique [1], Muhammad Imran Anwar [1,2,3], Masnita Misiran [1], Ilyas Khan [4,*], Asiful H. Seikh [5], El-Sayed M. Sherif [5,6] and Kottakkaran Sooppy Nisar [7]

1 School of Quantitative Sciences, Universiti Utara Malaysia, Sintok 06010, Malaysia; khurram.rafique1005@gmail.com (K.R.); imrananwar@uos.edu.pk (M.I.A.); masnita@uum.edu.my (M.M.)
2 Department of Mathematics, Faculty of Science, University of Sargodha, Sargodha 40100, Pakistan
3 Higher Education Department (HED), Lahore 54500, Pakistan
4 Faculty of Mathematics and Statistics, Ton Duc Thang University, Ho Chi Minh City 72915, Vietnam
5 Center of Excellence for Research in Engineering Materials (CEREM), King Saud University, P.O. Box 800, Al-Riyadh 11421, Saudi Arabia; aseikh@ksu.edu.sa (A.H.S.); esherif@ksu.edu.sa (E.-S.M.S.)
6 Electrochemistry and Corrosion Laboratory, Department of Physical Chemistry, National Research Centre, El-Behoth St. 33, Dokki, Cairo 12622, Egypt
7 Department of Mathematics, College of Arts and Sciences, Prince Sattam bin Abdulaziz University, Wadi Al-Dawaser 11991, Saudi Arabia; n.sooppy@psau.edu.sa
* Correspondence: ilyaskhan@tdtu.edu.vn

Received: 5 October 2019; Accepted: 27 November 2019; Published: 4 December 2019



Abstract: Brownian motion and thermophoresis diffusions are the fundamental ideas of abnormal upgrading in thermal conductivity via binary fluids (base fluid along with nanoparticles). The influence of Brownian motion and thermophoresis are focused on in the Buongiorno model. In this problem, we considered the Buongiorno model with Brownian motion and thermophoretic effects. The nonlinear ordinary differential equations are recovered from the partial differential equations of the boundary flow via compatible similarity transformations and then employed to the Keller-box scheme for numerical results. The physical quantities of our concern including skin friction, Nusselt number, and Sherwood number along with velocity, temperature and concentration profile against involved effects are demonstrated. The impacts of the involved flow parameters are drawn in graphs and tabulated forms. The inclination effect shows an inverse relation with the velocity field. Moreover, the velocity profile increases with the growth of the buoyancy effect.

Keywords: Keller-Box method; micropolar nanofluid; MHD; power law fluid; inclined surface

1. Introduction

Nanofluids set up a subclass of atomic liquids intended to work at the nanoscale. Nanofluids constitute the relation between bulk materials and molecular structure. The fast development of nanotechnology has witnessed exceptional attention in such liquids through the whole breadth of manufacturing, including engineering, aerospace, medical productions, and energy technologies. Nanofluid is a mix of various nanoparticles, for example, aluminum, silver, copper, and titanium with or without their oxides and base liquids, including water, ethylene glycol, oil, and so on. When nanoparticles strategically disperse in the base fluids, the resulting nanofluids have been confirmed to attain significant improvement in the properties of thermal conductivity presented by Choi [1]. The factors that play an important role in upgrading the thermal conductivity of nanofluid have been studied by Buongiorno [2]. Nanofluid flow over an inclined surface was reviewed by Sandeep and Kumar [3]. They investigated energy and mass

transport of dusty nanoparticles enhanced because of the volume fraction. Suriyakumar and Devi [4] studied the effects of internal heat generation and suction on mixed convective nanofluid flow through slanted surfaces. They found that the increment in the volume fraction of the copper water nanofluid diminishes the velocity field. Ziaei-Rad et al. [5] inspected the similarity solution of the boundary layer nanofluid flow over an inclined surface. They found that the energy transport increases with increasing the suction. Rashad [6] studied nanofluid flow by considering convective boundaries. Mitra [7] investigated computational modeling of nanofluid flow over an inclined surface. He concluded that the boundary layer thickness diminishes with the increase in inclination. Hatami et al. [8] discussed three-dimensional steady nanofluid over an inclined disk. For detailed literature about the flow of nanofluid with different geometries, see references [9–14].

The boundary layer flow over an inclined stretching surface becomes an interesting field of research because of its uses in designing, for example, paper production, skin grating, grain storage, and drag creation. The investigation of boundary layer flow over a steady surface was performed by Sakiadis [15]. Moreover, Crane [16] extended the work of Sakiadis [15] by studying the closed-form solution of boundary layer flow over an extending sheet. The boundary layer flow of dusty liquid over a slanted surface with heat source/sink was displayed by Ramesh et al. [17]. Singh [18] investigated the energy exchange of viscid liquid on a penetrable slanted surface numerically. A similarity solution of a magnetohydrodynmaic flow over an inclined sheet was calculated by Ali et al. [19]. Ramesh et al. [20] worked on the boundary layer flow towards an inclined surface. They considered the convective boundaries. The boundary layer-free convection flow over an inclined porous surface was scrutinized by Malik [21]. Hayat et al. [22] investigated the radiation effect on the flow produced by the stretching cylinder. Balla et al. [23] examined an inclined spongy cavity packed with nanofluid saturated in permeable medium.

Micropolar fluids are those which comprise of firm arbitrarily-oriented elements immersed in a sticky moderate with microstructure constituents, where distortion of the particle is unnoticed. Eringen [24] established a new philosophy of micropolar fluid to check the impact of micro-rotations on liquid movement. Rahman et al. [25] scrutinized the flow of micropolar liquid by incorporating the variable properties. They concluded from the results that the velocity profile shows an inverse correspondence with the inclination effect. The flow of micropolar fluid over an inclined surface with different effects has been studied by Das [26]. He discussed the energy and mass transport in this article. Kasim et al. [27] examined the micropolar fluid flow on the inclined plate numerically. Srinivasacharya and Bindu [28] explored how micropolar liquid moves through a slanted channel having parallel plates. Hazbavi and Sharhani [29] examined the flow of micropolar liquid among corresponding plates with a consistent pressure gradient. Rafique et al. [30] studied the heat and mass exchange of micropolar nanofluid fluid flow on a slanted surface. The effect of dual dispersion on micropolar liquid flow over a slanted surface was discussed by Srinivasacharya et al. [31]. Recently, Rafique et al. [32] probed the energy and mass transport of micropolar nanofluid flow over an inclined stretching surface. They found that the velocity profile diminishes with the increment in the inclination and magnetic effect. For the latest literature on micropolar fluid flow over an inclined surface, see [33–35].

In the light of the above-stated literature and its applications in engineering, it is the basis of motivation to scrutinize the inclination impact on micropolar nanofluid flow passed over an inclined nonlinear stretching surface. To the best of the author's knowledge, the inclination effect along with the magnetic field on the flow of micropolar nanofluid towards an inclined nonlinear stretching surface has not been yet reported. The current study is conducted to fulfill this gap. Suitable similarities transformations are utilized to recover the ordinary differential equations. The attained system of equations is then elucidated via the Keller-box scheme of Anwar et al. [36]. The Keller-box technique has been widely applied because it is the most flexible as compared to other approaches. It is informal to practice, much quicker, friendly to program, and effective.

2. Problem Formulation

Here we focus on the micropolar type nanofluid flow over an inclined surface by considering an angle γ. Where, $u_w(x) = ax^m$ is the extending speed, and $u_\infty(x) = 0$ is free stream speed in which x is the coordinate stately towards the extending sheet and 'a' is considered as constant. The transverse magnetic field $B(x) = B_0 x^{\frac{m-1}{2}}$ is taken normal to the stretching sheet with strength B_0. It is supposed that the electric and magnetic field properties are very insignificant as the magnetic Reynolds number is less, according to Mishra et al. [37]. The micropolar finite-size particles, along with Nanoparticles, are constantly distributed in the base fluids. The fluid particles have extra space to travel about formerly hitting the other fluid particles, where these particles revolve in the fluid field and fallouts for spinning effects in the micropolar nanofluid. The temperature T and nanoparticle fraction C take the values T_w and C_w at the wall, while the encompassing structures for nanofluid temperature and mass divisions T_∞ and C_∞ are achieved as y keeps an eye on infinity (see Figure 1).

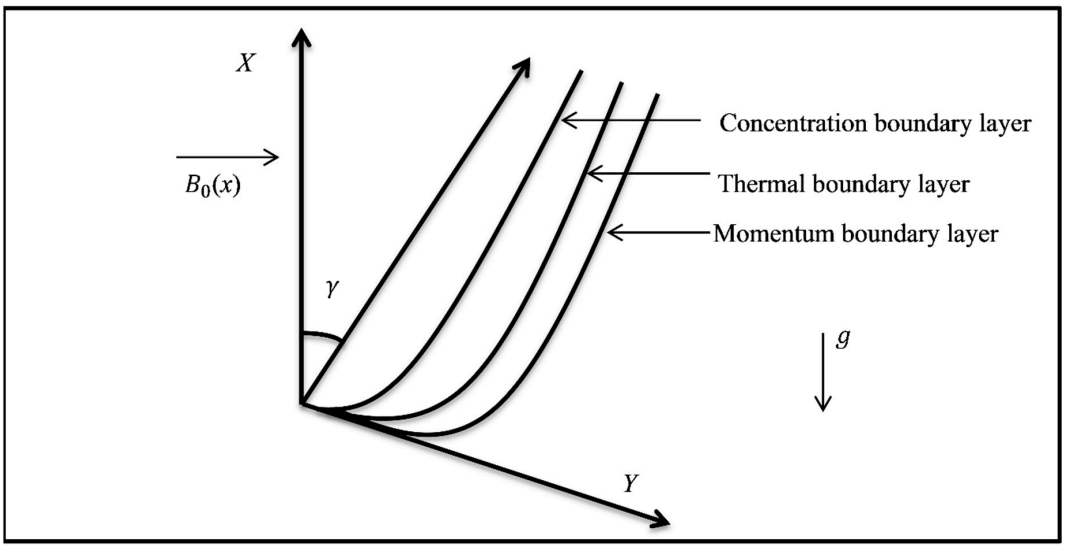

Figure 1. Physical geometry with coordinate system.

The governing equations for the problem under study are:

$$\frac{\partial u}{\partial x} + \frac{\partial v}{\partial y} = 0, \tag{1}$$

$$u\frac{\partial u}{\partial x} + v\frac{\partial u}{\partial y} = \left(\frac{\mu + K_1^*}{\rho}\right)\frac{\partial^2 u}{\partial y^2} + \left(\frac{K_1^*}{\rho}\right)\frac{\partial N^*}{\partial y} + g[\beta_t(T - T_\infty) + \beta_c(C - C_\infty)]cos\gamma - \frac{\sigma B^2(x)}{\rho}u, \tag{2}$$

$$u\frac{\partial N^*}{\partial x} + v\frac{\partial N^*}{\partial y} = \left(\frac{\gamma^*}{j^*\rho}\right)\frac{\partial^2 N^*}{\partial y^2} - \left(\frac{{K_1}^*}{j^*\rho}\right)\left(2N^* + \frac{\partial u}{\partial y}\right), \tag{3}$$

$$u\frac{\partial T}{\partial x} + v\frac{\partial T}{\partial y} = \alpha\frac{\partial^2 T}{\partial y^2} + \tau\left[D_B\frac{\partial C}{\partial y}\frac{\partial T}{\partial y} + \frac{D_T}{T_\infty}\left(\frac{\partial T}{\partial y}\right)^2\right], \tag{4}$$

$$u\frac{\partial C}{\partial x} + v\frac{\partial C}{\partial y} = D_B\frac{\partial^2 C}{\partial y^2} + \frac{D_T}{T_\infty}\frac{\partial^2 T}{\partial y^2}, \tag{5}$$

where in the directions x and y, the velocity constituents are u and v, individually, g is the gravitational acceleration, the uniform magnetic field strength is given by B_0, σ denotes the electrical conductivity, the viscosity is denoted by μ, the density of the base liquid is given by ρ_f, the density of the nanoparticle is given by ρ_p, the vortex viscosity is defined as k_1^*, the factor of thermal increase is given by β_t, β_c denotes the constant of concentration extension, the gyration ascent viscosity is given by γ^*, the micro

inertia each component mass is given by j^*, the micro-rotation is given by N^*, D_B denote the Brownian dispersal factor, D_T denotes the thermophoresis dispersion amount, $(\rho c)_p$ signifies the heat capacity of the nanoparticles, $(\rho c)_f$ represents the heat capacity of the conventional liquid, the thermal diffusivity parameter is denoted by $\alpha = \frac{k}{(\rho c)_f}$, and the relation between the active heat capacity of the nanoparticle and heat capacity of the liquid is represented by $\tau = \frac{(\rho c)_p}{(\rho c)_f}$.

The boundary settings in for concern problem are:

$$u = u_w(x) = ax^m,\ v = 0\ ,\ T = T_w\ ,\ N^* = -m_0\frac{\partial u}{\partial y}\ , C = C_w\ at\ y = 0,$$

$$u \to u_\infty(x) = 0,\ v \to 0\ ,\ T \to T_\infty\ , N^* \to 0,\ C \to C_\infty\ at\ y \to \infty. \tag{6}$$

The nonlinear ordinary differential equations are obtained from nonlinear partial differential equations. The stream function $\psi = \psi(x, y)$ for that purpose is given as

$$u = \frac{\partial \psi}{\partial y},\ v = -\frac{\partial \psi}{\partial x}. \tag{7}$$

For this study, the transformations are demarcated as:

$$\psi = \sqrt{\frac{2\nu a x^{m+1}}{m+1}} f(\eta),\ \theta(\eta) = \frac{T - T_\infty}{T_w - T_\infty},$$

$$\phi(\eta) = \frac{C - C_\infty}{C_w - C_\infty},\ \eta = y\sqrt{\frac{(m+1)ax^{m-1}}{2\nu}}. \tag{8}$$

$$N^* = ax^m\sqrt{\frac{a(m+1)x^{m-1}}{2v}}\ h(\eta),\ \mathrm{u} = \ \mathrm{a}x^m f\prime(\eta),$$

where $V = -\sqrt{\frac{av(m+1)x^{m-1}}{2}}\left[f(\eta) + \frac{m+1}{m-1}\eta f'(\eta)\right]$,

The Equations (2) to (5) are converted to the following nonlinear ordinary differential equations by utilizing Equation (8):

$$(1+K)f''' + ff'' - \left(\frac{2m}{m+1}\right)f'^2 + Kh' + \frac{2}{m+1}(Gr_x\theta + Gc_x\phi)cos\gamma - \frac{2}{m+1}Mf\prime = 0, \tag{9}$$

$$\left(1 + \frac{K}{2}\right)h'' + fh' - \frac{3m-1}{m+1}f'h - \frac{2K}{m+1}(2h + f'') = 0, \tag{10}$$

$$\left(\frac{1}{Pr}\right)\theta'' + f\theta' + Nb\phi'\theta' + Nt\theta'^2 = 0, \tag{11}$$

$$\phi'' + Le\phi' + Nt_b\theta'' = 0, \tag{12}$$

where,

$$M = \frac{\sigma B_0^2}{a\rho},\ Le = \frac{\nu}{D_B}, Pr = \frac{\nu}{\alpha},\ N_b = \frac{\tau D_B(C_w - C_\infty)}{\nu},\ N_t = \frac{\tau D_t(T_w - T_\infty)}{\nu T_\infty},\ K = \frac{k_1^*}{\mu},$$

$$Gr_x = \frac{g\beta_t(T_w - T_\infty)\ x^{-2m+1}}{a^2},\ Re_x = \frac{u_w(x)x}{\nu},\ Gc_x = \frac{g\beta_c(C_w - C_\infty)\ x^{-2m+1}}{a^2},\ Nt_b = \frac{N_t}{N_b}. \tag{13}$$

Here, primes mean the differentiation concerning η, the magnetic parameter is given by M, ν is kinematic viscosity, Pr is the Prandtl number, Gr_x denotes the local Grashof number, and Gc_x signifies the local modified Grashof number; to achieve the true similarity solution, the parameters Gr_x *and* Gc_x

must be constant. This condition is achieved if the thermal expansion coefficient β_t and concentration expansion coefficient β_c are proportional to x^{2m-1}. Hence, we assume that (see references [38–40])

$$\beta_t = nx^{2m-1},\ \beta_c = n_1 x^{2m-1}. \tag{14}$$

where n and n_1 are constants. Substituting Equation (14) in to the parameters Gr_x and Gc_x, we get

$$Gr = \frac{gn(T_w - T_\infty)}{a^2} \text{ and } Gc = \frac{gn_1(C_w - C_\infty)}{a^2}, \tag{15}$$

The transformed boundary conditions are

$$f(\eta) = 0,\ f'(\eta) = 1,\ h(\eta) = 0,\ \theta(\eta) = 1,\ \phi(\eta) = 1,\ at\ \eta = 0,$$

$$f'(\eta) \to 0,\ h(\eta) \to 0,\ \theta(\eta) \to 0,\ \phi(\eta) \to 0\ as\ \eta \to \infty, \tag{16}$$

It is found that by eliminating the vertex viscosity ($K = 0$), the situation agrees with a nanofluid model deprived of micropolar properties. The physical quantities for the current study are demarcated as

$$Nu_x = \frac{xq_w}{k(T_w - T_\infty)},\ Sh_x = \frac{xq_m}{D_B(C_w - C_\infty)},\ C_f = \frac{t_w}{{u_w}^2 \rho_f}, \tag{17}$$

where

$$q_w = -k\frac{\partial T}{\partial y},\ q_m = -D_B\frac{\partial C}{\partial y},\ \tau_w = \left(\mu + k_1^*\right)\frac{\partial u}{\partial y} + k_1^* N^*,\ at\ y = 0.$$

The associated terms for $C_{fx}(0) = (1+K)f''(0), -\theta(0), -\phi'(0)$, are denoted as

$$C_{fx}(0) = \frac{C_f}{2}\sqrt{\frac{2}{m+1}Re_x},\ -\theta'(0) = \frac{Nu}{\sqrt{Re_x\left(\frac{m+1}{2}\right)}},\ -\phi'(0) = \frac{Sh}{\sqrt{Re_x\left(\frac{m+1}{2}\right)}}, \tag{18}$$

where $Re_x = \frac{u_w(x)x}{\nu}$ represents the local Reynolds number.

3. Results and Discussion

This part demonstrates the numerical outcomes of the present study in the form of tables and graphs against involved parameters for different physical quantities. Table 1 is prepared for the authentication of the current outcomes with available results of Khan and Pop [41]. The outcomes are proven to have good agreement. Table 2 reveals the numerical outcomes of $-\theta'(0)$, $-\phi'(0)$, and $C_{fx}(0)$, against altered magnitudes of Nb, Nt, M, K, Gr, Gc, γ, m, Le, and Pr. It is clearly seen from Table 2 that $-\theta'(0)$ decreases with the growth of Nb, Nt, M, Le, m, *and* γ, and increases against K, Gr, Gc, and Pr. In addition, $-\phi'(0)$ upsurges on improving Nb, Gr, Gc, Nt, Le, K, *and* Pr and diminishes on enhancing M, m, and γ. In the same vein, $C_{fx}(0)$ upturns by increasing Le, M, K, Pr, γ, and m, and falls with the growth of Nt, Gr, Gc, and Nb.

Table 1. Results of $-\theta'(0)$ and $-\phi'(0)$ when M, K, Gr, $Gc = 0$, with $m = 1$, Pr = $Le = 10$ and $\gamma = 90°$.

Nb	*Nt*	Khan and Pop [41]		Present Results	
		$-\theta'(0)$	$-\phi'(0)$	$-\theta'(0)$	$-\phi'(0)$
0.1	0.1	0.9524	2.1294	0.9524	2.1294
0.2	0.2	0.3654	2.5152	0.3654	2.5152
0.3	0.3	0.1355	2.6088	0.1355	2.6088
0.4	0.4	0.0495	2.6038	0.0495	2.6038
0.5	0.5	0.0179	2.5731	0.0179	2.5731

Table 2. Numerical values of $-\theta\prime(0)$, $-\phi\prime(0)$ and $C_{fx}(0)$.

Nb	*Nt*	*Pr*	*Le*	*M*	*K*	*Gr*	*Gc*	*m*	γ	$-\theta'(0)$	$-\phi'(0)$	$C_{fx}(0)$
0.1	0.1	7.0	5.0	0.1	1.0	1.0	0.9	0.5	45^0	1.1618	1.2482	0.6326
0.5	0.1	7.0	5.0	0.1	1.0	1.0	0.9	0.5	45^0	0.2147	1.7428	0.6065
0.1	**0.5**	7.0	5.0	0.1	1.0	1.0	0.9	0.5	45^0	0.5199	1.9167	0.3007
0.1	0.1	**10.0**	5.0	0.1	1.0	1.0	0.9	0.5	45^0	1.1902	1.2594	0.6514
0.1	0.1	7.0	**10.0**	0.1	1.0	1.0	0.9	0.5	45^0	1.0231	2.2201	0.7370
0.1	0.1	7.0	5.0	**0.5**	1.0	1.0	0.9	0.5	45^0	1.1458	1.1979	0.9755
0.1	0.1	7.0	5.0	0.1	**5.0**	1.0	0.9	0.5	45^0	1.1744	1.3052	1.3112
0.1	0.1	7.0	5.0	0.1	1.0	**3.0**	0.9	0.5	45^0	1.1823	1.2887	0.0514
0.1	0.1	7.0	5.0	0.1	1.0	1.0	**2.0**	0.5	45^0	1.1783	1.2864	0.2174
0.1	0.1	7.0	5.0	0.1	1.0	1.0	0.9	**5.0**	45^0	1.1251	1.1644	1.5270
0.1	0.1	7.0	5.0	0.1	1.0	1.0	0.9	0.5	$\mathbf{90^0}$	1.1345	1.1862	1.3003

Figure 2 gives a picture of the upshot of factor M on $f\prime(\eta)$. The velocity outline slow down as we upsurge the constraint M. This is because the use of a magnetic field yields a Lorentz force, by means of which retards the fluid motion. A similar result has been seen in the instance of angular velocity against changed values of M in Figure 3. The variations in material parameter K show the velocity profile upturn (see Figure 4). The variation in angular velocity against the material parameter is portrayed in Figure 5. Clearly $h(\eta)$ increases with growing magnitudes of K on matching with the Newtonian case ($K = 0$); also, the boundary layer thickness reduces with the growth of K. The velocity shape upturns in Figure 6 by enhancing Grashof number Gr. Physically, the growing magnitude of the Grashof number declines with the viscous force that offers a favor to the fluid flow, which causes faster motion. Moreover, a similar result for the local modified Grashof number Gc on velocity disruption is prominent in Figure 7. Physically, the length, concentration difference and kinematic viscosity of the fluid affected the parameter Gc. On the other hand, there is an inverse relation between the viscosity and velocity of the fluid. Therefore, the viscosity of the fluid declines with the growing magnitude of Gc, and the concentration upsurges directly due to which the velocity field rises. Finally, the factor Gc shows a direct relation with the velocity outline. Figure 8 portrays the consequence of γ on $f\prime(\eta)$. It is demonstrated that the velocity outline depreciates as we enhance the values of inclination parameter γ. This can be ascribed to the circumstance that when the inclination parameter $\gamma = 0$ the gravitational force acting on the flow will be on the peak. Whereas, for $\gamma = 90^0$, the velocity profile diminishes due to the weaker bouncy forces. Similarly, the velocity profile shows an inverse relation with m, as depicted in Figure 9.

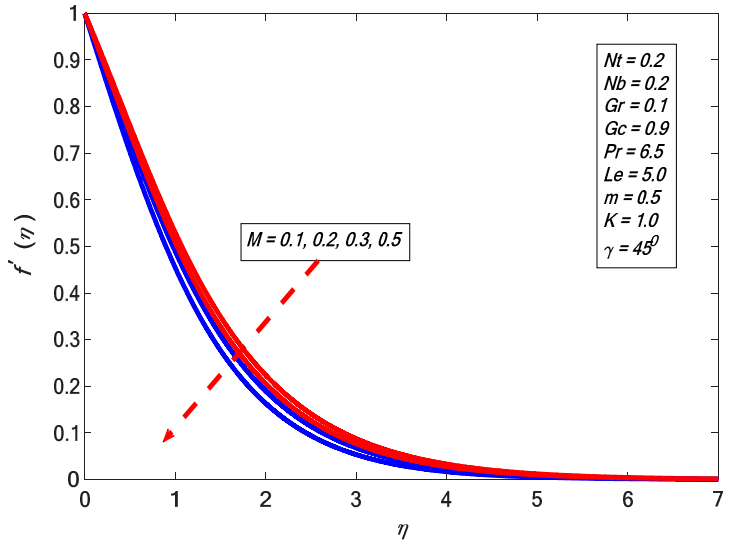

Figure 2. $f\prime(\eta)$ versus M.

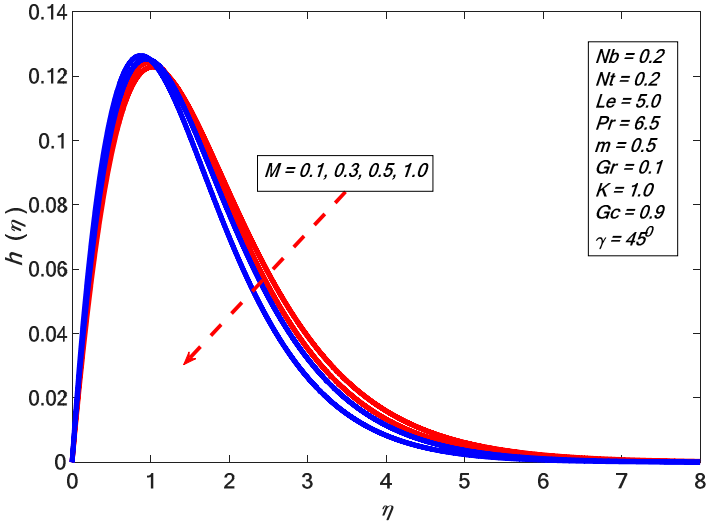

Figure 3. $h(\eta)$ versus M.

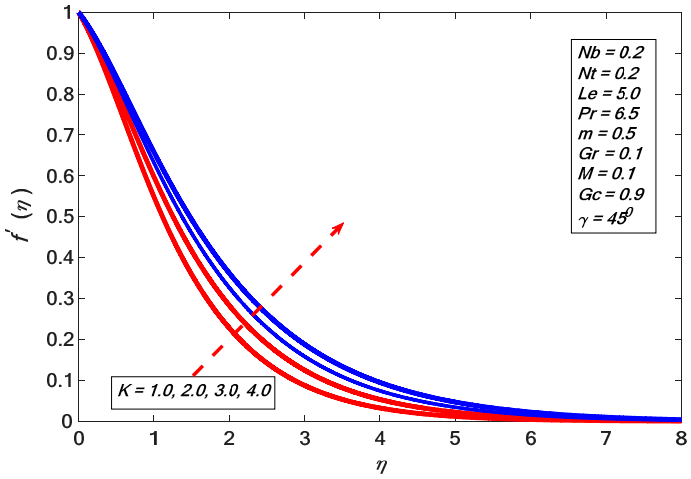

Figure 4. $f\prime(\eta)$ versus K.

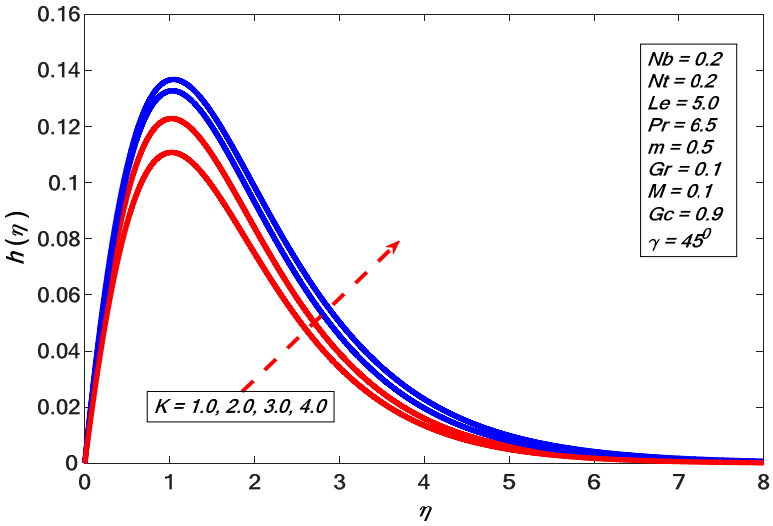

Figure 5. $h(\eta)$ versus K.

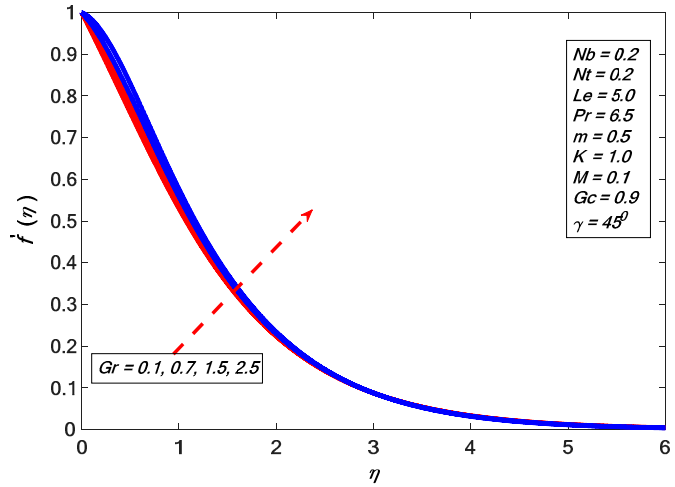

Figure 6. $f\prime(\eta)$ versus Gr.

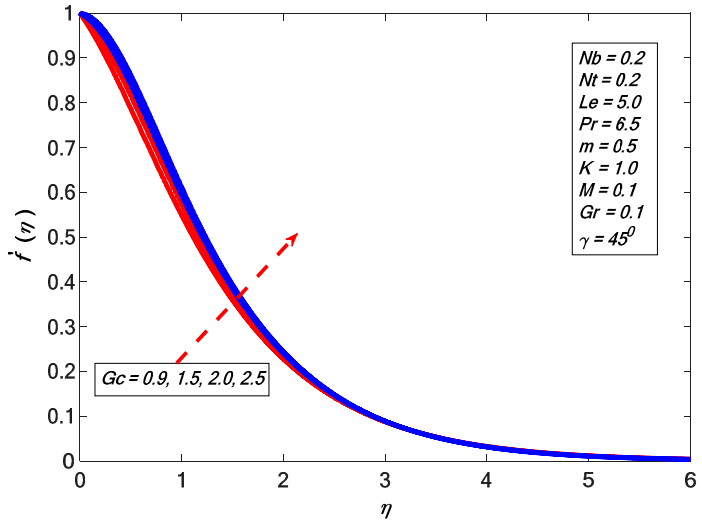

Figure 7. $f\prime(\eta)$ versus Gc.

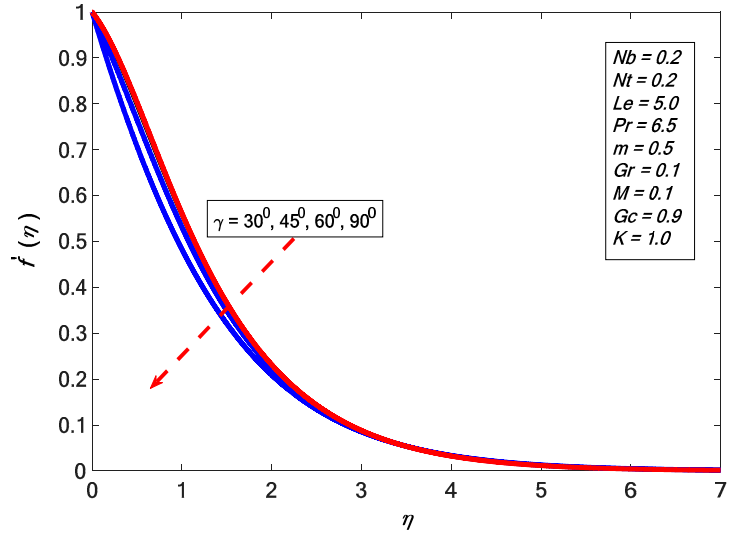

Figure 8. $f\prime(\eta)$ versus γ.

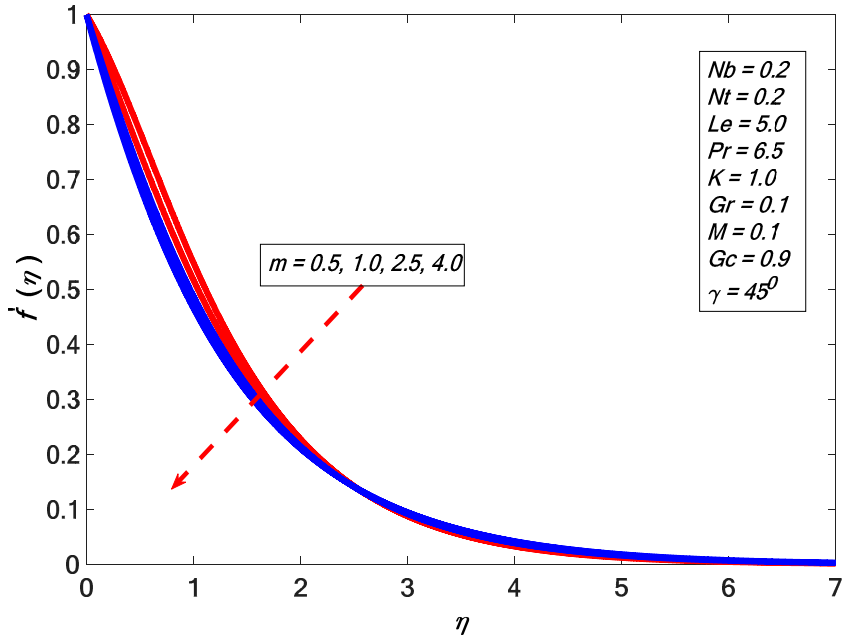

Figure 9. $f\prime(\eta)$ versus m.

Figures 10 and 11 display the of effect of Nb on $\theta(\eta)$ and $\phi(\eta)$ respectively. $\theta(\eta)$ increases with increasing Nb, whereas, $\phi(\eta)$ shows inverse behavior. Physically, Brownian motion warms the boundary layer which inclines to travel nanoparticles from the stretching surface to the fluid at rest, due to which the concentration of nanoparticles declines.

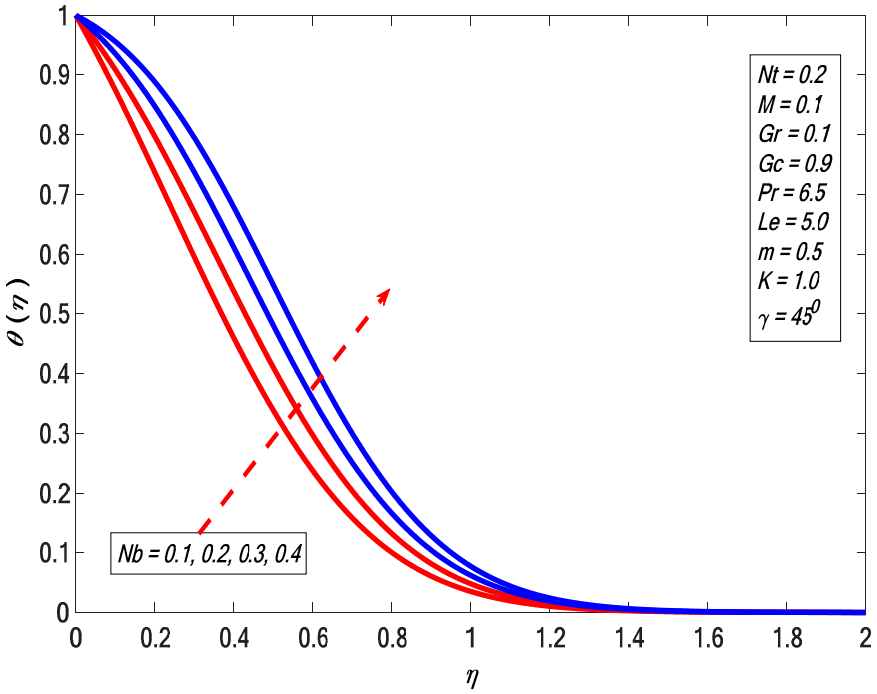

Figure 10. $\theta(\eta)$ versus Nb.

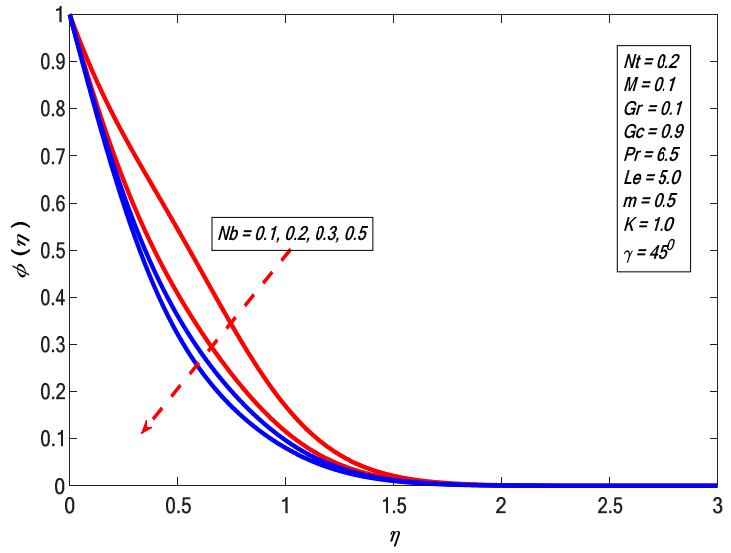

Figure 11. $\phi(\eta)$ versus Nb.

Figures 12 and 13 present $\theta(\eta)$ and $\phi(\eta)$ against several magnitudes of Nt. It is observed that both $\theta(\eta)$ and $\phi(\eta)$ increase by enhancing Nt. Thermophoresis works to heat up the boundary layer against several values of Prandtl and Lewis numbers. Besides the amount of heat and mass exchange reduced by improving thermophoresis constraint Nt. Figure 14 reveals that by growing the values of Pr, $\theta(\eta)$ drops, the reason behind this is the lessening of the thermal boundary layer viscosity by increasing Pr. In other words, an improvement in Pr means slowing the extent of thermal dispersion. Figure 15 displays the result of Lewis number Le on concentration profile. The boundary layer viscosity lessens by improving the values of Lewis number Le.

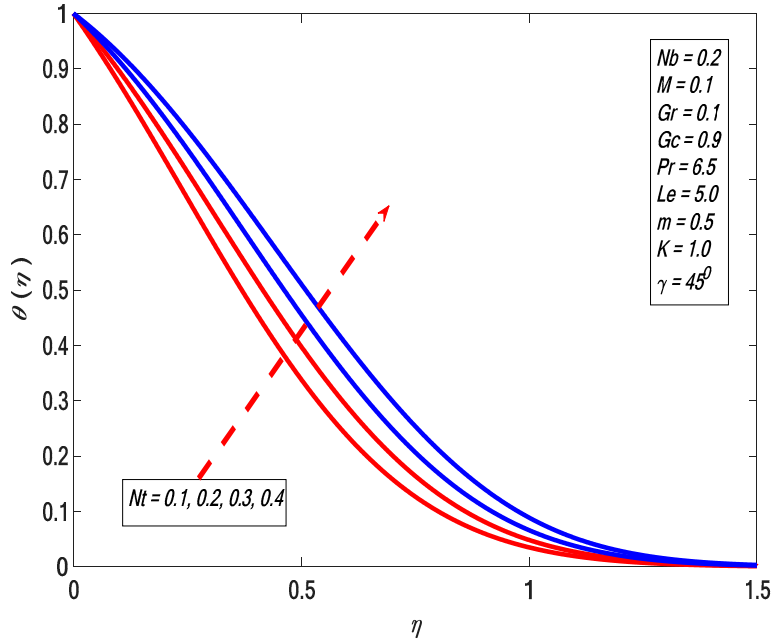

Figure 12. $\theta(\eta)$ versus Nt.

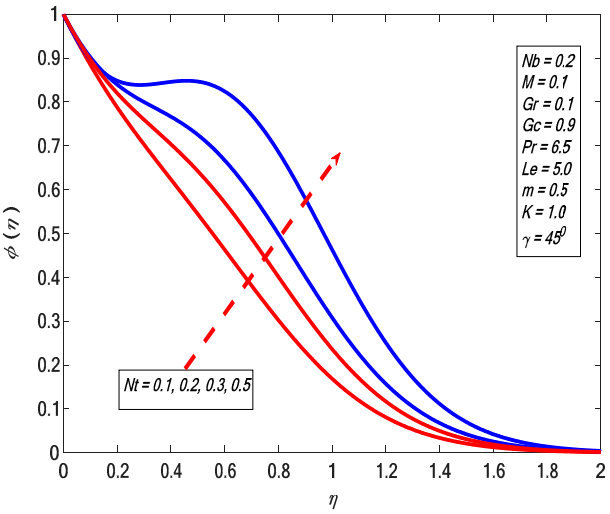

Figure 13. $\phi(\eta)$ versus Nt.

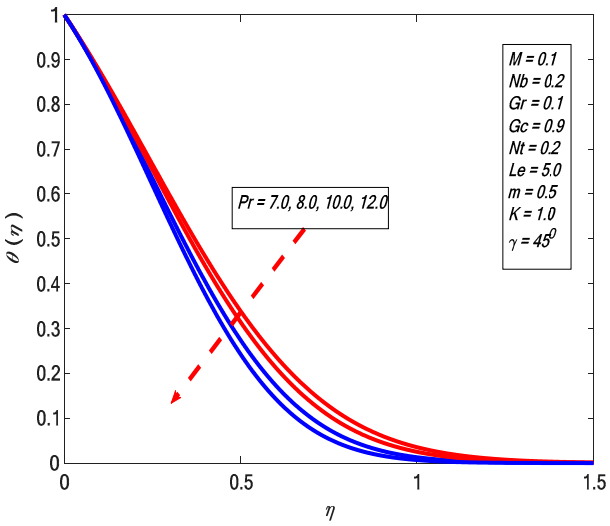

Figure 14. $\theta(\eta)$ versus Pr.

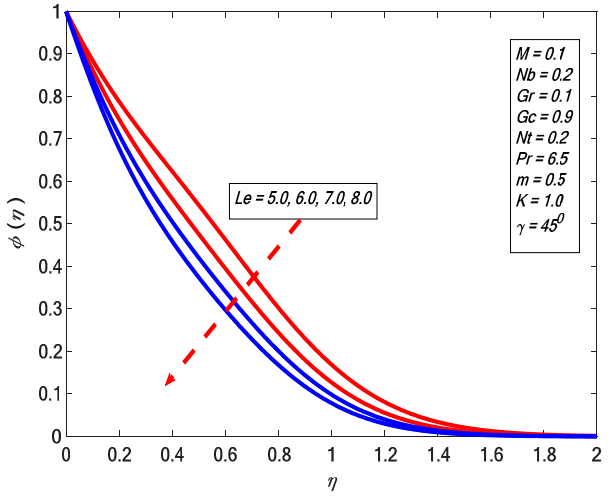

Figure 15. $\phi(\eta)$ versus Le.

4. Conclusions

Energy and mass transport of micropolar type nanofluid flow over a nonlinear inclined stretching surface with a magnetic field effect is examined. For numerical simulation, the Keller box scheme is employed. Table 1 is prepared for the validation of our current outcomes with already available literature. This type of study plays an important role in industry and engineering fields such as cooling of metallic plates, extrusion of polymers, nuclear reactors, electric devices and fiber construction. The key conclusions of the problems under concern are as follows:

- ➢ The velocity profile reduces by strengthening the magnetic field.
- ➢ The inclination effect diminishes $f\prime(\eta)$ for higher values.
- ➢ The Grashof number boosts the velocity profile.
- ➢ The heat and mass exchange rate are decreased with the growth of the inclination effect.
- ➢ The mass flux improves against the cumulative values of the Brownian motion factor.
- ➢ The wall shear stress decreases with the growth of the Brownian motion effect.

Author Contributions: Formulation done by K.R. and M.M. Problem solved by K.R. and M.I.A. Results computed by K.R.; I.K. and A.H.S. Results discussed by E.-S.M.S. and K.S.N. All authors contributed equally in writing manuscript.

Funding: The authors would like to extend their sincere appreciation to the Deanship of Scientific Research at King Saud University for its funding of this research through the Research Group Project No. RGP-160.

Acknowledgments: The authors would like to extend their sincere appreciation to the Deanship of Scientific Research at King Saud University for its funding of this research through the Research Group Project No. RGP-160.

Conflicts of Interest: The authors declare no conflict of interest.

Nomenclature

C_f	Skin friction coefficient	a	Stretching rate	Re_x	Reynolds number
C_∞	Ambient nanoparticle volume fraction	Le	Lewis number	Sh	Sherwood number
C_w	Surface volume fraction	Nb	Brownian motion parameter	T	Fluid temperature
c_p	Specific heat at constant pressure	Nt	Thermophoretic parameter	T_w	Wall temperature
D_B	Brownian diffusion coefficient	Nu	Nusselt number	T_∞	Ambient temperature
D_T	Thermophoretic diffusion coefficient	Pr	Prandtl number	u_w	Wall velocity
f	Similarity function for velocity	g	Gravitational acceleration	u_∞	Ambient velocity
ρc_p	Volume heat capacity	μ	Kinematic viscosity	ν	Dynamic viscosity
ϕ	Dimensionless solid volume fraction	w	Condition at the wall	∞	Ambient condition
Gc	Local modified Grashof number	β_t	Thermal expansion coefficient	β_c	Concentration expansion coefficient
σ	Electric conductivity	γ^*	Spin gradient viscosity	k_1^*	Vertex viscosity
j^*	Micro inertia per unit mass	γ	Inclination parameter	$'$	Differentiation with respect to η
u	Velocity in x direction	v	Velocity in y direction	x	Cartesian coordinate
θ	Dimensionless temperature	m	Non-linear stretching parameter	k	Thermal conductivity
ρ	Fluid density	Gr	Grashof number	B_0	Uniform magnetic field strength
K	Material parameter	η	Similarity independent variable	α	Thermal diffusivity
N^*	Non-dimensional angular velocity	C	Fluid concentration		

References

1. Choi, S.U.S.; Singer, D.A.; Wang, H.P. Developments and applications of non-Newtonian flows. *ASME FED* **1995**, *66*, 99–105.
2. Buongiorno, J. Convective transport in nanofluids. *J. Heat Transf.* **2006**, *128*, 240–250. [CrossRef]
3. Sandeep, N.; Kumar, M.S. Heat and Mass Transfer in Nanofluid Flow over an Inclined Stretching Sheet with Volume Fraction of Dust and Nanoparticles. *J. Appl. Fluid Mech.* **2006**, *9*, 2205–2215.
4. Suriyakumar, P.; Devi, S.A. Effects of Suction and Internal Heat Generation on Hydromagnetic Mixed Convective Nanofluid Flow over an Inclined Stretching Plate. *Eur. J. Adv. Eng. Technol.* **2015**, *2*, 51–58.
5. Ziaei-Rad, M.; Kasaeipoor, A.; Rashidi, M.M.; Lorenzini, G. A Similarity Solution for Mixed-Convection Boundary Layer Nanofluid Flow on an Inclined Permeable Surface. *J. Therm. Sci. Eng. Appl.* **2017**. [CrossRef]
6. Rashad, A. Unsteady nanofluid flow over an inclined stretching surface with convective boundary condition and anisotropic slip impact. *Int. J. Heat Technol.* **2017**, *35*, 82–90. [CrossRef]

7. Mitra, A. Computational Modelling of Boundary-Layer Flow of a Nano fluid Over a Convective Heated Inclined Plate. *J. Mech. Contin. Math. Sci.* **2018**, *13*, 88–94.
8. Hatami, M.; Jing, D.; Yousif, M.A. Three-dimensional analysis of condensation nanofluid film on an inclined rotating disk by efficient analytical methods. *Arab J. Basic Appl. Sci.* **2018**, *25*, 28–37. [CrossRef]
9. Rafique, K.; Anwar, M.I.; Misiran, M.; Khan, I.; Alharbi, S.O.; Thounthong, P.; Nisar, K.S. Numerical Solution of Casson Nanofluid Flow Over a Non-linear Inclined Surface With Soret and Dufour Effects by Keller-Box Method. *Front. Phys.* **2019**. [CrossRef]
10. Khan, M.; Shahid, A.; Malik, M.Y.; Salahuddin, T. Thermal and concentration diffusion in Jeffery nanofluid flow over an inclined stretching sheet: A generalized Fourier's and Fick's perspective. *J. Mol. Liq.* **2018**, *251*, 7–14.
11. Rafique, K.; Anwar, M.I.; Misiran, M. Keller-box study on casson nano fluid flow over a slanted permeable surface with chemical reaction. *Asian Res. J. Math.* **2019**, 1–17. [CrossRef]
12. Ghadikolaei, S.S.; Hosseinzadeh, K.; Ganji, D.D.; Jafari, B. Nonlinear thermal radiation effect on magneto Casson nanofluid flow with Joule heating effect over an inclined porous stretching sheet. *Case Stud. Therm. Eng.* **2018**, *12*, 176–187. [CrossRef]
13. Sheikholeslami, M. Numerical investigation of nanofluid free convection under the influence of electric field in a porous enclosure. *J. Mol. Liq.* **2018**, *249*, 1212–1221.
14. Mamun, A.A.; Arifuzzaman, S.M.; Reza-E-Rabbi, S.; Biswas, P.; Khan, M.S. Computational modelling on MHD radiative Sisko nanofluids flow through a nonlinearly stretching sheet. *Int. J. Heat Technol.* **2019**, *37*, 285–295. [CrossRef]
15. Sakiadis, B.C. Boundary-layer behavior on continuous solid surfaces: I. Boundary-layer equations for two-dimensional and axisymmetric flow. *AIChE J.* **1961**, *7*, 26–28.
16. Crane, L.J. Flow past a stretching plate. *Zeitschrift Für Angewandte Mathematik Und Physik (ZAMP)* **1970**, *21*, 645–647.
17. Ramesh, G.K.; Gireesha, B.J.; Bagewadi, C.S. Heat transfer in MHD dusty boundary layer flow over an inclined stretching sheet with non-uniform heat source/sink. *Adv. Math. Phys.* **2012**. [CrossRef]
18. Singh, P.K. Heat and mass transfer in MHD boundary layer flow past an inclined plate with viscous dissipation in porous medium. *Int. J. Sci. Eng. Res.* **2012**, *3*, 1–11.
19. Ali, M.; Alim, M.A.; Alam, M.S. Similarity Solution of Heat and Mass Transfer Flow over an Inclined Stretching Sheet with Viscous Dissipation and Constant Heat Flux in Presence of Magnetic Field. *Procedia Eng.* **2015**, *105*, 557–569. [CrossRef]
20. Ramesh, G.K.; Chamkha, A.J.; Gireesha, B.J. Boundary layer flow past an inclined stationary/moving flat plate with convective boundary condition. *Afr. Mat.* **2015**. [CrossRef]
21. Malik, M.Y.; Rehman, K.U. Effects of second order chemical reaction on MHD free convection dissipative fluid flow past an inclined porous surface by way of heat generation: A Lie group analysis. *Inf. Sci. Lett.* **2016**, *5*, 35–45. [CrossRef]
22. Hayat, T.; Qayyum, S.; Alsaedi, A.; Asghar, S. Radiation effects on the mixed convection flow induced by an inclined stretching cylinder with non-uniform heat source/sink. *PLoS ONE* **2017**, *12*, e0175584.
23. Balla, C.S.; Kishan, N.; Gorla, R.S.R.; Gireesha, B.J. MHD boundary layer flow and heat transfer in an inclined porous square cavity filled with nanofluids. *Ain Shams Eng. J.* **2017**, *8*, 237–254. [CrossRef]
24. Eringen, A.C. Simple microfluids. *Int. J. Eng. Sci.* **1964**, *2*, 205–217. [CrossRef]
25. Rahman, M.M.; Aziz, A.; Al-Lawatia, M.A. Heat transfer in micropolar fluid along an inclined permeable plate with variable fluid properties. *Int. J. Therm. Sci.* **2010**, *49*, 993–1002. [CrossRef]
26. Das, K. Slip effects on heat and mass transfer in MHD micropolar fluid flow over an inclined plate with thermal radiation and chemical reaction. *Int. J. Numer. Methods Fluids* **2012**, *70*, 96–113. [CrossRef]
27. Kasim, A.R.M.; Mohammad, N.F.; Shafie, S. Unsteady MHD mixed convection flow of a micropolar fluid along an inclined stretching plate. *Heat Transf. Asian Res.* **2013**, *42*, 89–99.
28. Srinivasacharya, D.; Bindu, K.H. Entropy generation in a micropolar fluid flow through an inclined channel. *Alex. Eng. J.* **2016**, *55*, 973–982. [CrossRef]
29. Hazbavi, A.; Sharhani, S. Micropolar fluid flow between two inclined parallel plates. In Proceedings of the ASME 2017 International Mechanical Engineering Congress and Exposition, Tampa, FL, USA, 3–9 November 2017.

30. Rafique, K.; Anwar, M.I.; Misiran, M.; Khan, I.; Seikh, A.H.; Sherif, E.S.M.; Nisar, K.S. Brownian Motion and Thermophoretic Diffusion Effects on Micropolar Type Nanofluid Flow with Soret and Dufour Impacts over an Inclined Sheet: Keller-Box Simulations. *Energies* **2019**, *12*, 4191. [CrossRef]
31. Srinivasacharya, D.; RamReddy, C.; Naveen, P. Double dispersion effect on nonlinear convective flow over an inclined plate in a micropolar fluid saturated non-Darcy porous medium. *Eng. Sci. Technol. Int. J.* **2018**, *21*, 984–995. [CrossRef]
32. Rafique, K.; Anwar, M.I.; Misiran, M. Numerical Study on Micropolar Nanofluid Flow over an Inclined Surface by Means of Keller-Box. *Asian J. Probab. Stat.* **2019**, 1–21. [CrossRef]
33. Arifuzzaman, S.; Mehedi, M.; Al Mamun, A.; Biswas, P.; Islam, M.; Khan, M. Magnetohydrodynamic micropolar fluid flow in presence of nanoparticles through porous plate: A numerical study. *Int. J. Heat Technol.* **2018**, *36*, 936–948. [CrossRef]
34. Shamshuddin, M.D.; Mishra, S.R.; Bég, O.A.; Kadir, A. Unsteady reactive magnetic radiative micropolar flow, heat and mass transfer from an inclined plate with joule heating: A model for magnetic polymer processing. *Proc. Inst. Mech. Eng. Part C J. Mech. Eng. Sci.* **2019**, *233*, 1246–1261. [CrossRef]
35. Rafique, K.; Anwar, M.I.; Misiran, M.; Khan, I.; Seikh, A.H.; Sherif, E.S.M.; Nisar, K.S. Numerical Analysis with Keller-Box Scheme for Stagnation Point Effect on Flow of Micropolar Nanofluid over an Inclined Surface. *Symmetry* **2019**, *11*, 1379. [CrossRef]
36. Anwar, M.I.; Shafie, S.; Hayat, T.; Shehzad, S.A.; Salleh, M.Z. Numerical study for MHD stagnation-point flow of a micropolar nanofluid towards a stretching sheet. *J. Braz. Soc. Mech. Sci. Eng.* **2017**, *39*, 89–100. [CrossRef]
37. Mishra, S.R.; Baag, S.; Mohapatra, D.K. Engineering Science and Technology, an International Journal Chemical reaction and Soret effects on hydromagnetic micropolar fluid along a stretching sheet. *Eng. Sci. Technol. Int. J.* **2016**, *19*, 1919–1928. [CrossRef]
38. Makinde, O.D.; Olanrewaju, P.O. Buoyancy effects on thermal boundary layer over a vertical plate with a convective surface boundary condition. *J. Fluids Eng.* **2010**, *132*, 044502. [CrossRef]
39. Ilias, M.R.; Rawi, N.A.; Shafie, S. MHD Free Convection Flow and Heat Transfer of Ferrofluids over a Vertical Flat Plate with Aligned and Transverse Magnetic Field. *Indian J. Sci. Technol.* **2016**, *9*, 36.
40. Olanrewaju, P.O.; Hayat, T. The effects of buoyancy and transpiration on the flow and heat transfer over a moving permeable surface in a parallel stream in the presence of radiation. *Int. J. Comput. Meth. Eng. Sci. Mech.* **2014**, *15*, 330–336. [CrossRef]
41. Khan, W.A.; Pop, I. Boundary-layer flow of a nanofluid past a stretching sheet. *Int. J. Heat Mass Transf.* **2010**, *53*, 2477–2483. [CrossRef]



© 2019 by the authors. Licensee MDPI, Basel, Switzerland. This article is an open access article distributed under the terms and conditions of the Creative Commons Attribution (CC BY) license (http://creativecommons.org/licenses/by/4.0/).